STEREO EVALUATION OF ALOS/PRISM DATA ON ESA-AO TEST SITES – FIRST DLR RESULTS

Mathias Schneider, Manfred Lehner, Rupert Müller, Peter Reinartz

German Aerospace Center (DLR), Remote Sensing Technology Institute, D-82234 Wessling, Germany
e-mail: {Mathias.Schneider, Manfred.Lehner, Rupert.Mueller, Peter.Reinartz}@dlr.de

ABSTRACT:

DLR's Remote Sensing Technology Institute has more than 20 years of history in developing spaceborne stereo scanners (MEOSS, MOMS) and the corresponding stereo evaluation software systems. It takes part in the ESA/JAXA-AO Program to evaluate the performance and potential of the three-line stereo scanner PRISM (Panchromatic Remote-sensing Instrument for Stereo Mapping) and the multispectral imaging sensor AVNIR-2 onboard the Japanese satellite ALOS as a principal investigator. French (near Marseille), German (near Munich) and Spanish (near Barcelona) test sites are proposed. In this paper, the process of direct georeferencing according to JAXA is shown and the results are presented. The geolocation accuracy improved immensely. For the newest dataset, ground control points (GCPs) are no longer obligatory, but useful. Rational polynomial coefficients (RPCs) are generated using DLR software. Thereby, oscillations in the orientation angles in the order of up to one pixel on the ground occurred in the older datasets. These oscillations can not be compensated by an RPC-based approach, however, in the newer dataset, they are no longer existent. The coregistration of forward, nadir and backward view is examined and DSMs are generated and analyzed.

1 INTRODUCTION

In the last years, the number of high resolution and very high resolution satellites increased and will further increase. For the orthorectification of the data gathered by these satellites, a digital elevation model (DEM) of sufficient accuracy is necessary. Up to now, the DEM produced by the Shuttle Radar Topography Mission (SRTM) is the best globally available DEM. However, with a resolution of 1-3 arc seconds, the potential of very high resolution imagery cannot be fully exploited. The PRISM instrument on the Japanese satellite ALOS combines high resolution imagery (2.5 m) with the capability to generate DEMs by providing three optical line scanners. Due to the experience of DLR's Remote Sensing Technology Institute (IMF) in developing spaceborne stereo scanners (MEOSS, MOMS) and the corresponding stereo evaluation software systems [7], processing chains for three-line scanners already exist that can be adapted to PRISM data. Also, RPC software was already developed [10]. In [6], orientation parameters are estimated using ground control points (GCPs) and self-calibration is performed. In [5], also a bundle adjustment is performed on the PRISM data.
In this paper, the DLR approach to orthorectify PRISM imagery and calculate digital surface models (DSM) from PRISM images is shown and first results are presented. For the processing, the image processing software XDIBIAS, developed at IMF, is used as well as a newly developed tool for the interpretation of PRISM housekeeping data.

2 THE PRISM INSTRUMENT

The PRISM instrument is one of three instruments onboard of the Japanese satellite ALOS (nickname “Daichi”) which was launched in January 2006. The other instruments are AVNIR-2, a multispectral radiometer, and PALSAR, a radar sensor. PRISM consists of three independent radiometers for nadir (N), backward (B) and forward (F) view. Each radiometer is composed of 6 (N) – 8 (F, B) CCD-arrays containing 4992 or 4928 pixels for nadir or forward/backward views respectively. There is a nominal overlap of 32 pixels between two neighboring CCD-arrays. Usually, an image is acquired using a subset of 4 consecutive CCD-arrays. The pixels, which are not used on the right and left CCD-array respectively, are regarded as so called dummy pixels and not used for the processing. A spatial resolution of 2.5 m is provided.
View angles of +/- 23.8 degree for forward and backward view with respect to the nadir view result in a base-to-height ratio of one [14]. In table 1, the characteristics of ALOS/PRISM are given. Fig. 1 shows the observation geometry of the PRISM instrument. For this paper, only the triplet mode was examined. A calibration/validation report is given in [13].

Table 1: Characteristics of ALOS/PRISM

Wavelength	0.52-0.77 micrometers (Panchromatic)
Base to height ratio	1.0 (between F and B view)
Resolution	2.5 m
Swath width	35 km in triplet mode
Pointing angle	-1.5 to 1.5 degree
Stereo angle	+/- 23.8 degree (F/B)
Flying height	691650 m
Focal length	1.939 m
Number of CCDs	6 (N)/8 (F/B)
Pixel per CCD array	4992 (N)/4928 (F/B)

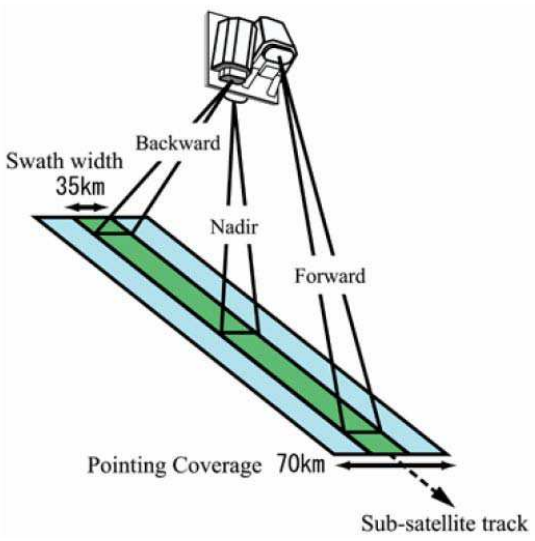

Figure 1: Observation geometry of triplet mode [14].

3 DATA FORMAT

PRISM data can be delivered in different stages of processing: Level 1A, where no correction is done, Level 1B1, where the images are radiometrically corrected and Level 1B2, where the images are radiometrically and geometrically corrected. Imagery and ancillary data are given in CEOS format, partly in ASCII and partly in binary code.

For our purposes, Level 1B1 data are the most suitable ones. Level 1A and 1B1 images are composed by one image file per CCD with an overlap of 32 pixels. The image is thus created by merging the 4 image files together and the overlap is accounted for by cutting off 16 pixels of the overlap area of each image file. The column number of the composed image is then 14496. The image data itself is JPEG compressed on board of the satellite. Compression artifacts are visible in the imagery. To minimize the artifacts, a filter can be applied. E.g., an image enhancement software can be downloaded at [4]. We applied a 3x3 Gaussian filter before matching the images, which increases the quality of the matching results.

The imaging time for each line is given in the image files, while the ancillary data needed for our purposes is written in the SUP- file. According to [1], the following data are extracted: Precision orbit (ancillary 8), precision attitude (ancillary 12), coordinate conversion matrices (ancillary 10) and geometric parameter (ancillary 13).

4 DATA

Different test datasets are used. One test site is located near Barcelona in Catalonia, Spain. Beside two sets (F, N, B) of PRISM L1B1 images, 5 orthophotos, provided by the Institut Cartográfic de Catalunya (ICC), are available for GCP and ICP measurement as well as a digital terrain model DTM of the test site, also provided by ICC. The PRISM images were acquired in October 2006, ordered via ESA and therefore also processed by the ESA processor in April 2007. Unfortunately, the processor used at ESA was not updated when processing the data. Especially the parameters of the pointing alignment, which are used to calculate the interior orientation, have to be updated, before an efficient use of the data.

Therefore, a second test data set was provided by GAEL Consultant. The PRISM L1B1 images show the coastal region of Marseille in the south of France and were acquired in March 2007. The coordinates of six GCPs were provided, measured with GPS, as well as a DSM with 1 arc second resolution provided by SPOT Image. This PRISM dataset was processed at JAXA with the JAXA processor in October 2007.

The third dataset is newer, so that most of the parameters are improved. The third test site is located near Munich in Germany. Beside the PRISM images, 5 orthophotos are available as well as a SRTM-DSM of the area. The PRISM images were acquired in June 2007 and processed in September 2008 by the ESA processor.

5 DIRECT GEOREFERENCING

Unlike other papers (e.g. [6]), we tried to follow the processing given in [2] and [3]. Therefore, in the first step, the view vector u_{CCD} for each pixel in the CCD coordinate system is calculated as follows:

$$u_{CCD} = \frac{1}{\sqrt{1+dx^2+dy^2}} \begin{pmatrix} dx \\ dy \\ 1 \end{pmatrix} \quad (1)$$

where

$$dx = \tan(\theta_Y(k))$$
$$dy = -\tan(\theta_X(k)) \quad (2)$$

and

$$\theta_X(k) = \frac{k_2 - k}{k_2 - k_1}\theta_X(k_1) + \frac{k - k_1}{k_2 - k_1}\theta_X(k_2) + a_X\left(k - \frac{k_1 + k_2}{2}\right)^2 - b_X \quad (3)$$
$$\theta_Y(k) = \frac{k_2 - k}{k_2 - k_1}\theta_Y(k_1) + \frac{k - k_1}{k_2 - k_1}\theta_Y(k_2) + a_Y\left(k - \frac{k_1 + k_2}{2}\right)^2 - b_Y$$

k_1, k_2 are the pixel numbers at the measurement points, while k is the actual pixel number and is computed as follows:

$$k(i) = (CCD\_no - 1)(pix - 32) + left\_dummy\_pix + i \quad (4)$$

where pix = 4992 in case of a nadir image and
pix = 4928 for forward/backward view and

$$\theta_X(k_i) = \theta_{X0i} + \delta\theta_{X0i} \qquad \text{for i} = \{1,2\} \quad (5)$$
$$\theta_Y(k_i) = \theta_{Y0i} + \delta\theta_{Y0i}$$

The values for $k_i, \theta_{X0i}, \theta_{Y0i}, \delta\theta_{X0i}, \delta\theta_{Y0i}$ are retrieved from the SUP-file, ancillary 13, as well as the values for a_X, b_X, a_Y, b_Y, which account for the CCD distortion.
This view vector is then transformed to the earth centered rotated coordinate system (ECR) ITRF97 u_{ECR}.

$$u_{ECR} = QMAu_{CCD} \quad (6)$$

where $$Q = R_{XY}R_{GAST}R_{PN} \quad (7)$$

R_{XY} is built using the information for polar motion (XY-matrix part), R_{GAST} is built using the Greenwich Apparent Sidereal Time information and R_{PN} is built using the precession/nutation information (PN-matrix part). The needed information is given in the SUP-file, ancillary 10. Q is the matrix that transforms a vector from earth centered inertial coordinate system (ECI) J2000 to ECR.
Matrix M(q) is built using the quaternions from precision attitude, also given in the SUP-file (ancillary 12), as follows:

$$M(q) = \begin{pmatrix} 1-2(q_2^2+q_3^2) & 2(q_1q_2 - q_0q_3) & 2(q_1q_3 + q_0q_2) \\ 2(q_1q_2 + q_0q_3) & 1-2(q_1^2+q_3^2) & 2(q_2q_3 - q_0q_1) \\ 2(q_1q_3 - q_0q_2) & 2(q_2q_3 + q_0q_1) & 1-2(q_1^2+q_2^2) \end{pmatrix} \quad (8)$$

Roll pitch and yaw angles are extracted from M(q) as follows:

$$roll = -\arcsin(M_{23})$$
$$pitch = \arctan(\frac{M_{13}}{M_{33}}) \quad (9)$$
$$yaw = \arctan(\frac{M_{21}}{M_{22}})$$

The angles at imaging time are computed by linear interpolation. The matrix M at imaging time is then built as follows:

$$M = R_y(pitch)R_x(roll)R_z(yaw) \quad (10)$$

where

$$R_x(roll) = \begin{pmatrix} 1 & 0 & 0 \\ 0 & \cos(roll) & -\sin(roll) \\ 0 & \sin(roll) & \cos(roll) \end{pmatrix}$$
$$R_y(pitch) = \begin{pmatrix} \cos(pitch) & 0 & \sin(pitch) \\ 0 & 1 & 0 \\ -\sin(pitch) & 0 & \cos(pitch) \end{pmatrix} \quad (11)$$
$$R_z(yaw) = \begin{pmatrix} \cos(yaw) & -\sin(yaw) & 0 \\ \sin(yaw) & \cos(yaw) & 0 \\ 0 & 0 & 1 \end{pmatrix}$$

M is the matrix that transforms a vector from satellite coordinate system to ECI. The matrix A is built from various information given in the SUP-file, ancillary 13.

$$A = (n_0 A_{STT})^{-1}(nAn_0)^{-1}\Delta R(I,n) \quad (12)$$

where

$$n_0 A_{STT} = \begin{pmatrix} 1 & \psi nl & -\theta nl \\ -\psi nl & 1 & \phi nl \\ \theta nl & -\phi nl & 1 \end{pmatrix}\begin{pmatrix} an11 & an12 & an13 \\ an21 & an22 & an23 \\ an31 & an32 & an33 \end{pmatrix} \quad (13)$$

where the coefficients an11-an33 account for the mount angles of the optics, stereo angles, etc.. The coefficients in the first matrix represent the long period bias time variation by a linear expression of the number of days since the start date.

$$nAn_0 = \begin{pmatrix} 1 & \psi n & -\theta n \\ -\psi n & 1 & \phi n \\ \theta n & -\phi n & 1 \end{pmatrix} \quad (14)$$

where the coefficients are computed by a polynomial of degree 30 of the dimensionless number s, which normalizes the time, when the satellite is in sunshine, by the orbit period of 98.7 minutes. The polynomial coefficients are also given in the SUP-file, ancillary 13.

$$\Delta R(I,n) = \begin{pmatrix} 1 & \Psi(I,n) & -\theta(I,n) \\ -\Psi(I,n) & 1 & \phi(I,n) \\ \theta(I,n) & -\phi(I,n) & 1 \end{pmatrix} \quad (15)$$

where the coefficients are given for each CCD (n) and each radiometer (I) in the SUP-file, ancillary 13. The matrix eliminates the differences between CCD coordinate system defined in the PRISM sensor model and the reference CCD coordinate system for the pointing alignment parameters. However, in the test datasets, the coefficients were zero.

5.1 Interior Orientation

To use the existing programs at DLR, some modifications had to be made. Exterior and interior orientations have to be given for each line and each pixel respectively. Therefore, equation (6) is split up in two parts. The interior orientation has to be given in a table as view vector for each pixel according to equation (16).

$$u_{\text{int}} = Au_{CCD} \quad (16)$$

Additionally, an atmospheric correction has to be applied according to [3]:

$$\begin{pmatrix} vx' \\ vy' \\ vz' \end{pmatrix} = \frac{1}{\sqrt{\delta vx^2 + \delta vy^2 + vz^2}} \begin{pmatrix} \delta vx \\ \delta vy \\ vz \end{pmatrix} \quad (17)$$

where vx, vy, vz are the elements of u_{int} and

$$\delta = \frac{\tan(\theta - \Delta\theta)}{\tan\theta} \quad (18)$$

where

$$\theta = \tan^{-1}\frac{\sqrt{vx^2 + vy^2}}{vz} \quad (19)$$

and

$$\Delta\theta = 2.316\tan\theta\left(\frac{P_1 - P_2}{H} - 34.11\frac{P_2}{T}\right) + \delta_1 + \delta_2 \quad (20)$$

with

$$\delta_1 = \tan\theta\frac{2 + 3\tan^2\theta}{5}\delta_1' \quad (21)$$

and

$$\delta_2 = 0.129\tan\theta\frac{e_1 - e_2}{H} + 95\frac{e_2}{T} \quad (22)$$

where
H is the nominal satellite altitude in mm,
P_1 is the standard atmospheric pressure at ground in hPa,
P_2 is the atmospheric pressure at satellite altitude in hPa,
T is the atmospheric temperature at satellite altitude in K,
δ_1' is the earth curvature correction coefficient in radian,
e_1 is the vapour pressure at ground in hPa and
e_2 is the vapour pressure at satellite altitude in hPa.
To be compatible with the existing DLR software, the sign of the z-component of the view vector is changed and the vector is normalized so that the z-component is 1 for each pixel.

5.2 Exterior Orientation

The exterior orientation consists of the angles for roll, pitch and yaw and of the satellite position at imaging time in ECR coordinates. This information has to be given for each imaging line. The angles are extracted from the first part of equation (6), the product of Q and M, as described in equation (9). Since in the existing DLR programs, the definition of the direction of the rotation is different, the signs of the extracted angles are changed.
The satellite position and velocity is given as precision orbit data in the SUP-file, ancillary 8, both in ECI and ECR coordinates for every minute. Both position and velocity at imaging time are calculated using a Hermite interpolation, considering the 4 data points around the point of interest.
Due to the non-infinite velocity of light, the velocity of the satellite and the velocity of a point on the earth surface cause pixel location errors. To account for this effect, equation 23 is applied.

$$u'_{ECR} = \frac{u_{ECR} - \frac{v_{POD}}{c}}{\left|u_{ECR} - \frac{v_{POD}}{c}\right|} \quad (23)$$

Where v_{POD} is the satellite velocity at imaging time and c is the velocity of light. Since this correction is applied on the view vector in the ECR coordinate system, it was integrated in the existing DLR software ORTHO [12].

5.3 Focal Point Offset

Due to the size of the satellite, the offset between the three focal points for backward, nadir and forward radiometers and the satellite mass center has to be accounted for and is not negligible as it is for most of the other satellites. The offset is given in ancillary 13 by three vectors that are added up. The result is shown in

table 2 and is used in the sensor configuration files that are needed in the different DLR software modules.

Table 2: Offset between focal points and satellite mass center

	Forward	Nadir	Backward
dx [m]	2.718	1.216	3.368
dy [m]	-0.2295	-0.0695	0.8575
dz [m]	0.450	-0.619	-0.179

5.4 Geolocation

Ground control points (GCPs) are measured in all images. The DLR developed software ESTIMATE is used to estimate boresight angles. As additional result, ESTIMATE returns the RMS values at the GCPs before the improvement. Table 3 shows the results for the different test regions.

Table 3: RMS values at GCPs

		RMSx [pixel]	RMSy [pixel]
Catalonia 25 GCP	F	8.187	7.929
	N	90.282	15.936
	B	38.763	15.988
Marseille 6 GCP	F	23.405	9.525
	N	32.604	2.331
	B	4.927	7.168
Bavaria 33 GCP	F	4.787	3.246
	N	6.631	3.191
	B	2.712	1.071

Due to the improved parameters, especially in ancillary 13, the location accuracy improved immensely. For the older datasets the use of GCPs is inevitable whereas for the newest dataset – depending on the desired accuracy – an orthorectification or DEM generation without GCPs is possible.
In the following tests, we used the GCPs to estimate boresight angles.

5.5 RPC Generation

Since for a RPC-based approach no new software had to be developed, the first idea was to generate RPCs for the PRISM images. Therefore, a three dimensional grid of control points is generated over the whole image from the exterior and interior orientation. This is done by a modification of the software ORTHO, developed at DLR [12]. The previously estimated boresight angles are used as input for ORTHO.
The RPCs are then computed as described in [11], using XDIBIAS RPC generation software, developed at DLR. To check the RPCs, coordinates of the control points were recalculated using the RPCs and compared to the original coordinates. Fig. 2 shows the plot of these residual vectors for a nadir image of a test site in Catalonia/Spain.
The results are similar for forward and backward images as well as for the test site near Marseille. The residuals are smaller than one pixel; however, they may affect the DEM-generation.

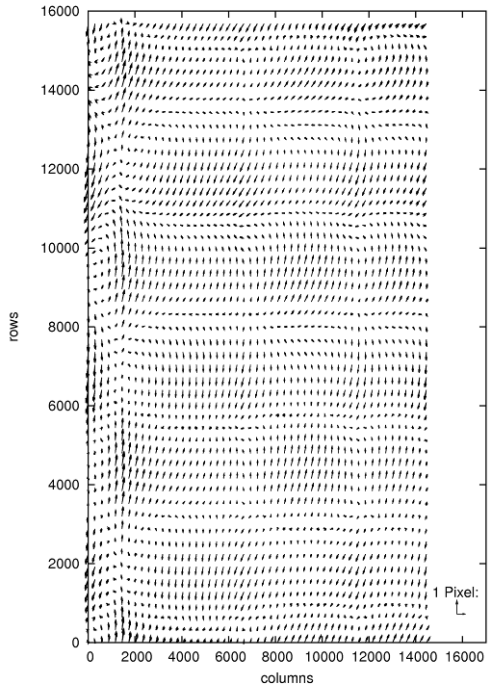

Figure 2: Residuals between original control point coordinates and those calculated by RPCs for nadir image of Catalonian test site.

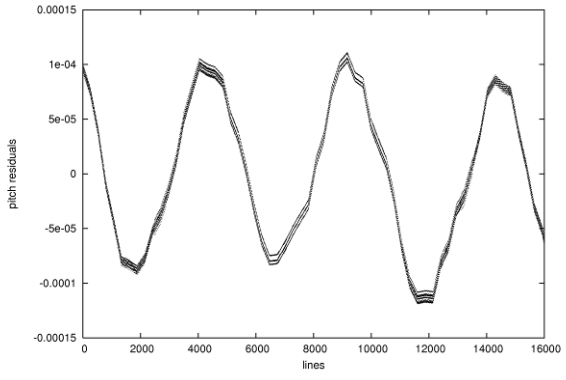

Figure 3: Residuals of pitch angle after subtracting a second degree polynomial for nadir image of Catalonian test site. Values are in degree.

Regarding the residual behavior in row direction, there seems to be an oscillation with an amplitude of approximately one pixel. In order to find the reason for this oscillation, the attitude angles are examined.
When plotting the attitude angles for an image, they seem to have a linear behavior. However, when we estimate a second degree Legendre polynomial as trend line and subtract it from the original values, an oscillation is clearly visible. Fig. 3 shows the residuals in pitch angle for the nadir view of the test site in Catalonia/Spain. The amplitude of the oscillation is small; however, in the images, it results in deviations of up to one pixel. For the yaw angle, the plot looks similarly, while for the roll angles, the residuals are slightly smaller.
However, when analyzing the newest dataset in Bavaria/Germany, this oscillation is no longer visible as can be seen in Fig. 4.

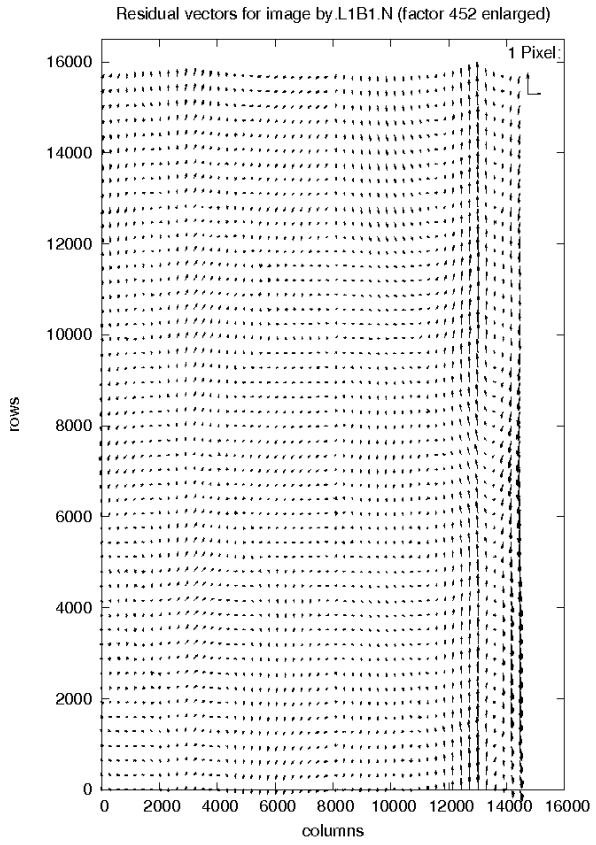

Figure 4: Residuals between original control point coordinates and those calculated by RPCs for nadir image of German test site.

The transition between the CCDs can still be seen in this plot; however, the displacements are smaller than half a pixel.
The absence of the oscillation in the newest dataset might either be caused by the improved sensor model, or the oscillation might be caused by something that does not occur permanently. Maybe it is caused by PALSAR working at the same time, or the oscillation may result from vibrations caused by satellite steering, etc. Similar oscillations are also known from other cases, e.g. MOMS-2P [8].
Since the reason for the oscillation is still unknown, this effect has to be examined further in the future.
In case that the oscillation also occurs in newly processed datasets, the RPC-based approach is not suitable for PRISM imagery, since the effects can not be handled by RPCs. Then the rigorous model should be used.
In case that the oscillation was eliminated by the improved parameters and does not occur any more, the RPC-based model can be used.

6 STEREO PROCESSING

For the moment, the RPC approach was chosen, knowing that the oscillation described in chapter 5.5 will occur in the older datasets.

6.1 Forward, Nadir and Backward Co-Registration

For the German test site, orthoimages are produced using DLR developed orthoprocessing software ORTHO. A SRTM-based DSM is used for the orthorectification as well as 33 GCPs derived from orthophotos that were available for this test area. The GCPs were used to estimate boresight angles that were introduced into the orthorectification process.
After the orthorectification of the images, an overlay of nadir and backward view is created. Fig. 5 shows a part of this overlay.

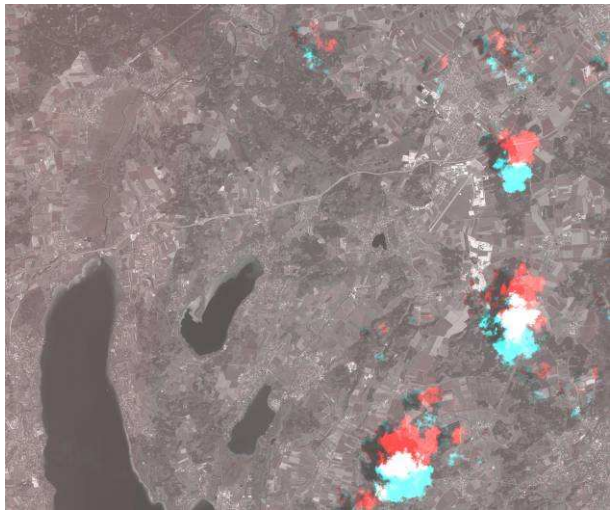

Figure 5: Overlay of nadir and backward view. Blue and green channel show the nadir view whereas the red channel shows the backward view.

The predominant grey color indicates a very good coregistration. Major differences can only be detected at the clouds that are not orthorectified and probably moved between the acquisitions of the two images. Small differences occur also at buildings due to the different viewing angles of nadir and backward camera. Also, a matching – originally developed for MOMS and MEOSS imagery ([7], [9]) and further enhanced since then – between nadir and backward orthoimages was performed to display the quality of the coregistration of nadir and backward view. In the result, no systematic effects are visible, the differences are very small. As can be seen in table 4, the statistics on the matching points also indicate a very good coregistration. The results for the nadir/forward comparison are very similar.

Table 4: Statistics on 108478 matching points nadir/backward, values are given in pixels.

	Row	Column
Min	-5.14	-1.64
Max	4.40	3.08
Mean	-1.16	0.57
Std.-dev.	0.64	0.41

6.2 DSM Generation

For the Catalonian test site, a DSM is calculated using the RPC-based approach. Therefore, after a matching of forward, nadir and backward image, a forward intersection is computed for the tie points. Three and two ray points are used. A DSM is then interpolated from the resulting mass points.

The DSM is then compared to the reference DTM provided by ICC. Figures 6 and 7 show this comparison across and in flight direction, respectively. The profiles show a very good correlation both in position and in height.

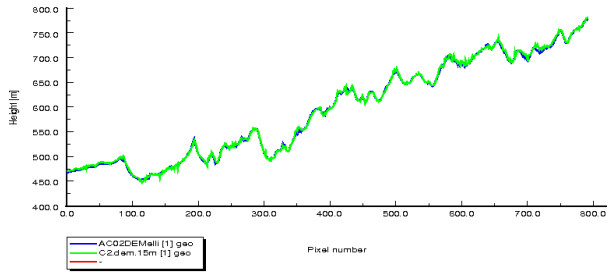

Figure 6: Comparison of a profile in PRISM DSM (green) and reference DTM (blue) in the north-western part of the images. The profile is across-track.

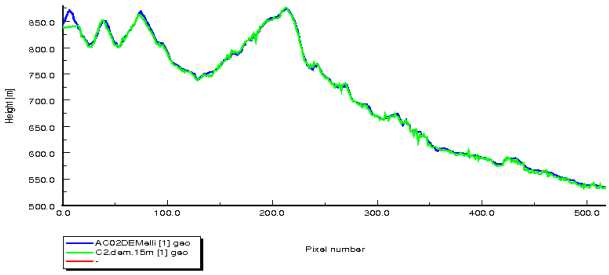

Figure 7: Comparison of a profile in PRISM DSM (green) and reference DTM (blue) in the northern part of the images. The profile is along-track.

Due to the immense amount of points and the resulting size of the files, the processing is done in eight chips. When merging these chips to one DSM, differences may occur in the overlapping areas, especially in areas where only few points are found, e.g. in dense forests or in large agricultural areas. This effect worsens the overall statistics shown in table 5. Therefore, the statistics are also calculated for the north-western DSM chip.

Table 5: Statistics on difference image between PRISM DSM and reference DTM for Catalonian test site, values are given in meters.

	Overall	Chip 1
Min	-134.430	-81.540
Max	277.740	93.040
Mean	0.936	-0.231
Std.-dev.	10.679	3.964

There are some few outliers, probably caused by mismatchings or interpolation artifacts; however, the mean difference is very small. Also the standard deviation is quite small, especially when regarding the chip. The DSMs for the French and German test sites deliver similar results. The remaining differences result from typical DSM generation problems, such as e.g. the difficulty to match points in areas with a uniform texture, and are not PRISM specific problems.

7 CONCLUSION

After extraction of ancillary data from ALOS PRISM files, orthoimages and DSMs can be created. In this paper, the way of direct georeferencing is shown, according to [2]. The results improved when using newly processed data with updated sensor model parameters. Tests showed that while for older datasets ground control points have to be used to estimate boresight angles, for the newer dataset orthorectification and DSM generation is possible without GCPs with an accuracy of 10 -15 m.

It is shown, that an RPC-based approach reveals an oscillation of up to one pixel in the image for the older datasets. While it might be tolerable for orthoimage generation for most applications, it will affect the DSM generation. In the newest dataset, the oscillation no longer exists, maybe due to the improved sensor model parameters. Another possible reason for the oscillation might be vibrations caused by some satellite part that is not working permanently, e.g. PALSAR. In case that the oscillation has permanently vanished, a RPC-based approach is applicable. If not, we recommend the use of a rigorous approach rather than a RPC-based approach. This has to be examined further in the future.

Coregistration tests of forward, nadir and backward orthoimages show a high correlation between the different views.

Comparison of PRISM DSM and reference DTM reveals a very high quality of the PRISM DSM. The differences between PRISM DSMs and reference DTMs are in the expected dimension.

After overcoming some difficulties and with the improved sensor model parameters, PRISM data are now a very valuable source for DSM generation with a good accuracy.

REFERENCES

1. JAXA, 2006a: ALOS PRISM Level 1 Product Format Descriptions Rev.J, October 2006. http://www.eorc.jaxa.jp/ALOS/doc/format.htm

2. JAXA, 2006b: ALOS Algorithm description (PRISM/AVNIR-2)

3. JAXA, 2007: PRISM sensor modelling and its parameters

4. Kamiya I., 2006: Study on ALOS PRISM, homepage: http://gisstar.gsi.go.jp/ALOS/index_e.html

5. Kamiya I., 2007: Geometric Characteristics of the Early Products of ALOS PRISM. Bulletin of the Geographical Survey Institute, vol.54, pp.75–82.

6. Kocaman S., Gruen A., 2007: Rigorous Sensor Modeling of ALOS/PRISM Imagery. 8th Conference on Optical 3D Measurement Techniques, Zurich, Switzerland, 9-12 July.

7. Kornus W., Lehner M. and Schroeder, M., 2000, Geometric inflight calibration by block adjustment using MOMS-2P 3-line-imagery of three intersecting stereo-strips, SFPT (Société Francaise de Photogrammétrie et Télédétection), Bulletin Nr. 159, pp. 42-54

8. Lehner M., Müller R., 2003. Quality Check of MOMS-2P Orthoimages of Semi-Arid Landscapes, Proceedings of ISPRS Worjshop on “High Resolution Mapping from Space 2003”, October 6-8, Hannover, Germany

9. Lehner M. and Gill R.S., 1992. Semi-automatic derivation of digital elevation models from stereoscopic 3-line scanner data, IAPRS, Vol. 29, Part B4, Washington, USA, pp. 68-75.

10. Lehner M., Müller Ru., Reinartz P., 2005: DSM and Orthoimages from QuickBird and Ikonos Data Using Rational Polynomial Functions, Proceedings of “High Resolution Earth Imaging for Geospatial Information”, May 17-20, Hannover, Germany

11. Lehner M., Müller R., Reinartz P., Schroeder M., 2007: Stereo evaluation of Cartosat-1 data for French and Catalonian test sites, Proceedings of the ISPRS Hannover Workshop 2007 High Resolution Earth Imaging for Geospatial Information, Hannover, Germany, May 29 – June 1

12. Müller, Ru.; Lehner, M.; Reinartz, P.; Schroeder, M.; 2005: “Evaluation of Spaceborne and Airborne Line Scanner Images using a generic Ortho Image Processor”, Proc. of High Resolution Earth Imaging for Geospatial Information, ISPRS Hannover Workshop, Commision I WG 5, 2005 http://www.ipi.uni-hannover.de/fileadmin/institut/pdf/046-mueller.pdf

13. Saunier S., Demange C., Goryl, P., 2007: Final calibration/validation report PRISM. http://earth.esa.int/pub/ESA_DOC/ALOS011.pdf

14. Tadono T., Shimada M., Watanabe M., Hashimoto T., Iwata T., 2004: Calibration and Validation of PRISM Onboard ALOS. International Archives of Photogrammetry, Remote Sensing and Spatial Information Sciences, Vol.XXXV part B1, pp. 13-18.

ACKNOWLEDGEMENTS

The authors would like to thank Sébastien Saunier of GAEL Consultants for his advice and providing a test dataset, Dr. Wolfgang Kornus of ICC for providing ground truth for the Catalonian test site and Marc Bernard of SPOT Image for providing a DEM for the French test site.